Efficient Inhibition of the Alzheimer's Disease ²-Secretase by Membrane Targeting

Lawrence Rajendran, *et al.*

Science **320**, 520 (2008);
DOI: 10.1126/science.1156609

Science (print ISSN 0036-8075; online ISSN 1095-9203) is published weekly, except the last week in December, by the American Association for the Advancement of Science, 1200 New York Avenue NW, Washington, DC 20005.

forcing is generally underestimated. This is consistent with other studies indicating that models undersimulate precipitation responses to external forcing (*13*–*16*, *23*).

The Arctic Oscillation (AO) is an important contributor to Northern Hemisphere climate variability (*1*, *3*). The prolonged positive AO phase during recent decades is in accord with precipitation changes over Europe and the Arctic (*3*, *24*, *25*). Although modeled AO responses to anthropogenic forcing are generally weaker than observed (*26*, *27*), some studies suggest anthropogenic influences may have been a factor (*9*). To test the sensitivity of our detection results to the possible effect of AO fluctuations, we repeated our detection analyses on observed precipitation series that exclude variability linearly related to the AO. We did so by linearly regressing the observed gridded monthly precipitation anomalies onto the AO index, defined as the first principal component of the monthly mean sea level pressure anomalies north of 20°N (*25*) and by retaining only the regression residuals for detection analyses. The detection results obtained in this way (Fig. 2B) are improved: The scaling factors are closer to one, and model-simulated variability agrees better with observed. This increases confidence in our detection result because it demonstrates human influence on aspects of Arctic precipitation change that are not related to a component of circulation change that has been associated with model structural uncertainty. Nevertheless, it remains difficult to assess the effects of model structural uncertainty, as well as that of observational uncertainty, on our results.

Our results indicate that anthropogenic forcing from greenhouse gases and sulfate aerosols combined has contributed to the observed high-latitude precipitation increase during the latter half of the 20th century. We also find that model-simulated precipitation responses to anthropogenic forcing are weaker than in the observations. This implies that model-projected future precipitation change may also be too weak, which would have important implications for the development of adaptation strategies: It is possible that future Arctic Ocean freshening and MOC slowdown could occur more quickly than indicated by currently available GCM simulations (*7*). Recent studies show that Arctic sea ice is declining substantially faster than indicated by model simulations (*28*, *29*).

References and Notes

1. R. E. Moritz, C. M. Bitz, E. J. Steig, *Science* **297**, 1497 (2002).
2. IPCC, *Climate Change 2007: Impacts, Adaptation and Vulnerability. Contribution of Working Group II to the Fourth Assessment Report of IPCC* (Cambridge Univ. Press, Cambridge, 2007).
3. ACIA, *Arctic Climate Impact Assessment: Scientific Report* (Cambridge Univ. Press, Cambridge, 2005).
4. S. Rahmstorf, *Nature* **419**, 207 (2002).
5. B. J. Peterson *et al.*, *Science* **298**, 2171 (2002).
6. K. E. Trenberth *et al.*, in *Climate Change 2007: The Physical Science Basis. Contribution of Working Group I to the Fourth Assessment Report of IPCC*, (Cambridge Univ. Press, Cambridge, 2007), pp. 235–336.
7. B. J. Peterson *et al.*, *Science* **313**, 1061 (2006).
8. G. A. Meehl *et al.*, in *Climate Change 2007: The Physical Science Basis. Contribution of Working Group I to the Fourth Assessment Report of IPCC* (Cambridge Univ. Press, Cambridge, 2007), pp. 747–845.
9. G. C. Hegerl *et al.*, in *Climate Change 2007: The Physical Science Basis. Contribution of Working Group I to the Fourth Assessment Report of IPCC* (Cambridge Univ. Press, Cambridge, 2007), pp. 663–745.
10. K. M. Willett, N. P. Gillett, P. D. Jones, P. W. Thorne, *Nature* **449**, 710 (2007).
11. B. D. Santer *et al.*, *Proc. Natl. Acad. Sci. U.S.A.* **104**, 15248 (2007).
12. M. R. Allen, W. J. Ingram, *Nature* **419**, 224 (2002).
13. F. H. Lambert, P. A. Stott, M. R. Allen, M. A. Palmer, *Geophys. Res. Lett.* **31**, 10203 (2004).
14. N. P. Gillett, A. J. Weaver, F. W. Zwiers, M. F. Wehner, *Geophys. Res. Lett.* **31**, 12217 (2004).
15. F. H. Lambert, N. P. Gillett, D. A. Stone, C. Huntingford, *Geophys. Res. Lett.* **32**, 18704 (2005).
16. X. Zhang *et al.*, *Nature* **448**, 461 (2007).
17. T. C. Peterson, R. S. Vose, *Bull. Am. Meteorol. Soc.* **78**, 2837 (1997).
18. Materials and methods are available as supporting material on *Science* Online.
19. G. Gruza, E. Rankova, V. Razuvaev, O. Bulygina, *Clim. Change* **42**, 219 (1999).
20. G. C. Hegerl *et al.*, *Clim. Dyn.* **13**, 613 (1997).
21. M. R. Allen, P. A. Stott, *Clim. Dyn.* **21**, 477 (2003).
22. M. R. Allen, S. F. B. Tett, *Clim. Dyn.* **15**, 419 (1999).
23. F. J. Wentz, L. Ricciardulli, K. Hilburn, C. Mears, *Science* **317**, 233 (2007).
24. D. W. J. Thompson, J. M. Wallace, *Science* **293**, 85 (2001).
25. D. W. J. Thompson, J. M. Wallace, G. C. Hegerl, *J. Clim.* **13**, 1018 (2000).
26. N. P. Gillett, *Nature* **437**, 496 (2005).
27. R. L. Miller, G. A. Schmidt, D. T. Shindell, *J. Geophys. Res.* **111**, D18101 (2006).
28. M. C. Serreze, M. M. Holland, J. Stroeve, *Science* **315**, 1533 (2007).
29. J. Stroeve, M. M. Holland, W. Meier, T. Scambos, M. Serreze, *Geophys. Res. Lett.* **34**, L09501 (2007).

30. We thank R. Vose and P. Ya. Groisman at the National Climatic Data Centre for the observed precipitation data, and P. Stott and T. Nozawa for the provision of model data. We are grateful to M. Mackay, W. Skinner, and two anonymous reviewers for their helpful comments. We acknowledge the modeling groups, the Program for Climate Model Diagnosis and Intercomparison (PCMDI), and the World Climate Research Programme's (WCRP) Working Group on Coupled Modelling (WGCM) for their roles in making available the WCRP CMIP3 multimodel data set. Support of this data set is provided by the Office of Science, U.S. Department of Energy. S.-K.M. is supported by the Canadian International Polar Year program.

Supporting Online Material

www.sciencemag.org/cgi/content/full/320/5875/518/DC1
Materials and Methods
SOM Text
Figs. S1 to S4
Tables S1 and S2
References

27 November 2007; accepted 18 March 2008
10.1126/science.1153468

Efficient Inhibition of the Alzheimer's Disease β-Secretase by Membrane Targeting

Lawrence Rajendran,[1] Anja Schneider,[2] Georg Schlechtingen,[3,4] Sebastian Weidlich,[4] Jonas Ries,[5] Tobias Braxmeier,[3,4] Petra Schwille,[5] Jörg B. Schulz,[6] Cornelia Schroeder,[4] Mikael Simons,[2] Gary Jennings,[3] Hans-Joachim Knölker,[3,4] Kai Simons[1]*

β-Secretase plays a critical role in β-amyloid formation and thus provides a therapeutic target for Alzheimer's disease. Inhibitor design has usually focused on active-site binding, neglecting the subcellular localization of active enzyme. We have addressed this issue by synthesizing a membrane-anchored version of a β-secretase transition-state inhibitor by linking it to a sterol moiety. Thus, we targeted the inhibitor to active β-secretase found in endosomes and also reduced the dimensionality of the inhibitor, increasing its local membrane concentration. This inhibitor reduced enzyme activity much more efficiently than did the free inhibitor in cultured cells and in vivo. In addition to effectively targeting β-secretase, this strategy could also be used in designing potent drugs against other membrane protein targets.

A key molecule in the pathogenesis of Alzheimer's disease (AD) is the β-amyloid peptide (Aβ), which, either in its soluble oligomeric form or in the plaque-associated version, leads to neurodegeneration (*1*). Aβ is liberated from the membrane-spanning β-amyloid precursor protein (APP) by sequential proteolytic processing using β- and γ-secretases. β-Secretase activity is conferred by a transmembrane aspartyl protease, also termed BACE-1 (β-amyloid cleaving enzyme 1), which catalyzes the rate-limiting reaction in the generation of Aβ (*2*). β-Secretase cleavage of APP occurs predominantly in endosomes, and endocytosis of APP and β-secretase is essential for β cleavage and Aβ production (*3*–*7*). The low pH of endosomes is optimal for β-secretase activity. Conversely, α-secretase cleavage of APP, which precludes production of the toxic Aβ peptide, occurs at the plasma membrane (*8*). Both β- and γ-secretase are thus propitious therapeutic targets (*1*, *9*). However, in

view of the multiple functions of γ-secretase, β-secretase might be the preferred therapeutic target (*10*).

Several transition-state inhibitors have been designed to block the active site of the β-secretase enzyme (*11*, *12*). Many of these have shown potent activity against the purified ectodomain of β-secretase or the reconstituted enzyme (*11*, *13*). Nonetheless, many fail in cellular assays (*14*, *15*). A critical issue in designing inhibitors against the enzyme is to direct inhibition to the subcellular compartment where the enzyme is active. Here, we tested the efficacy of a membrane-tethered version of an otherwise soluble inhibitor that is targeted to endosomes via endocytosis.

Endocytosis is essential for β-secretase activity (*3*–*7*); we thus tested whether the internalization of β-secretase inhibitors was needed for activity. To this end, we assayed the activity of a nonpermeable transition-state peptide inhibitor of β-secretase in a cellular assay, where the production of α-secretase, β-secretase–cleaved ectodomains of APP (sAPPα, sAPPβ, respectively) and Aβ was followed. The free inhibitor inhibited both recombinant and soluble β-secretase (*11*, *13*) (fig. S1) but failed to inhibit β cleavage in cells (Fig. 1 and fig. S2). Because most of the β cleavage occurs in endosomes (*3*–*7*, *16*), sufficient amounts of the free inhibitor might not reach this compartment.

We reasoned that membrane tethering would render the soluble inhibitor competent for endocytosis and deliver the inhibitor to endosomes. Hence, we coupled a sterol moiety as a membrane anchor via a polyglycol linker to the C terminus of the inhibitory peptide (fig. S3) via solid-phase synthesis (see supporting online material). On the basis of the length of the peptide cleavage domain of APP (β/A4 region of APP-770) (*17*), the appropriate length of the linker for inhibition of β-secretase was estimated to be about 89 Å. The sterol-linked inhibitor was more active than the free inhibitor in inhibiting β cleavage (Fig. 1, A and C) and Aβ production (Fig. 1D). Because the free inhibitor coupled to the polyglycol linker but lacking the sterol moiety was inactive, we concluded that the sterol moiety, not the polyglycol linker, was critical for effective β-secretase inhibition (fig. S4). Likewise, another control where the sterol group was N-terminally linked to the inhibitor was also inactive, ruling out a direct influence of the sterol moiety (Fig. 1, A and C). The failure of the N-terminally linked inhibitor to inhibit β-secretase also suggested that proper orientation of the inhibitory peptide was essential for inhibition. Similar results were obtained in a neuroblastoma cell line (fig. S5). Thus, membrane anchoring of an otherwise soluble inhibitor leads to a considerable increase in efficacy.

Having shown that the membrane-anchored inhibitor blocked β-secretase more efficiently than did the free inhibitor in cultured cells, we proceeded to demonstrate that the membrane-anchored inhibitor was indeed transported to the endosomes where β cleavage occurs. For this purpose, we synthesized a fluorescent derivative of both the sterol-linked and the free inhibitor. This labeled inhibitor was equally active against β-secretase (Fig. 2A) and was rapidly endocytosed (Fig. 2B). Inhibition of endocytosis through the use of a mutant dynamin (DynK44A) markedly reduced internalization of the inhibitor (Fig. 2C), whereas overexpression of either soluble green fluorescent protein (GFP; Fig. 2C) or wild-type dynamin (fig. S6) did not alter internalization of the inhibitor. The internalized inhibitor accumulated in endosomes that also harbored APP and BACE-1 (Fig. 2D), which showed that sterol-anchoring efficiently directed the inhibitor to endosomes. Concentrations as low as 0.1 μM were sufficient to block the appearance of the β-cleaved ectodomain of APP in the cells (Fig. 2, E and F) (*6*). In contrast, the free inhibitor was not internalized, nor did it inhibit the production of β-cleaved ectodomain (Fig. 2E). Although sterol-linked inhibitors decreased β cleavage of APP, they concomitantly increased α cleavage (Fig. 1, B and C, and fig. S4). Inhibition of endocytosis also produced the same effect (*3*, *4*, *8*), suggesting that membrane-anchored inhibitor targeted the active β-secretase in endosomes.

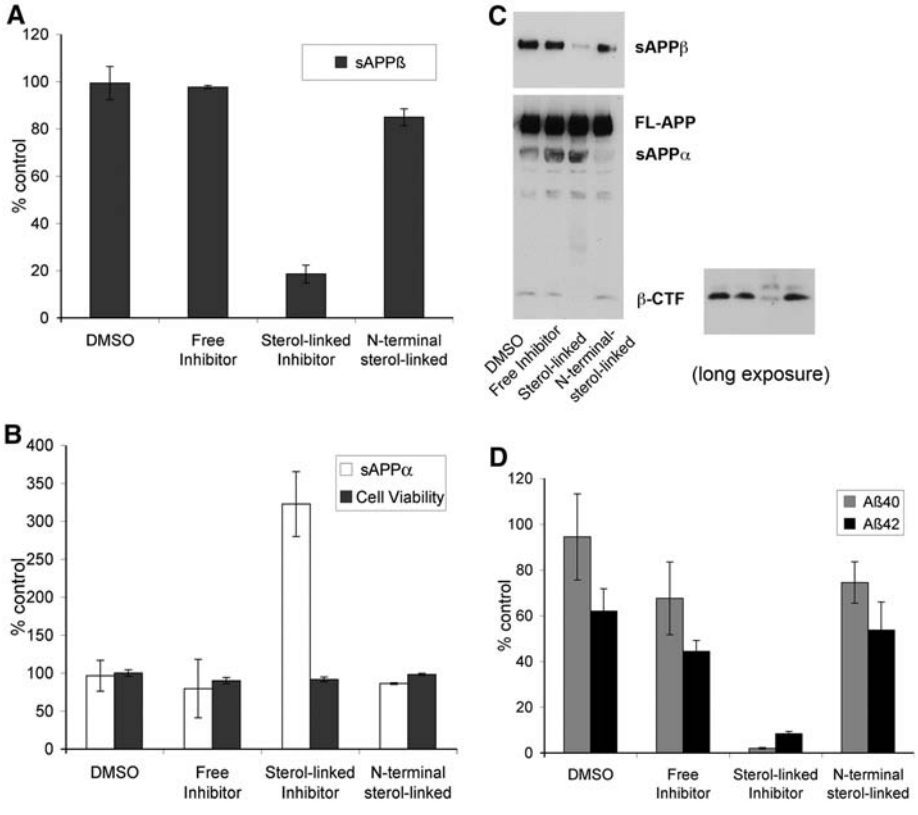

Fig. 1. Sterol-linked inhibitor inhibits β-secretase cleavage of APP and Aβ production. HeLa-swAPP cells were treated with test compounds (200 nM) and the medium was analyzed for (**A**) β cleavage (i.e., the β-cleaved ectodomain, sAPPβ) and (**B**) α cleavage (i.e., the α-cleaved ectodomain, sAPPα) by electrochemiluminescence (ECL) assay (*6*). Cell viability values in (B) are from Alamar Blue assay. (**C**) sAPPβ levels were detected by immunoblotting cell lysates from the samples, using the sAPPβ-specific antibody AN]] (*6*). Full-length APP (FL-APP), sAPPα, and β-cleaved C-terminal fragment (β-CTF) were analyzed by immunoblotting with 6E10 (lower and side panel). Longer exposure (side panel) reveals a clear reduction in β-CTF levels in the sterol-linked inhibitor lane. FL-APP levels serve as the loading control. (**D**) Sterol-linked inhibitor inhibited secretion of Aβ peptides (Aβ40, Aβ42) as measured by ECL assay. Inhibitor data are expressed with respect to DMSO control; DMSO data are expressed as percent-untreated control. ECL results shown are representative of more than four independent experiments and are expressed as means ± SD (sAPPβ, $P < 0.001$; Aβ40, $P = 0.008$; Aβ42, $P = 0.01$; sAPPα, $P = 0.003$).

[1]Max Planck Institute of Molecular Cell Biology and Genetics, Pfotenhauerstr. 108, 01307 Dresden, Germany. [2]Max Planck Institute for Experimental Medicine, 37075 Göttingen, Germany. [3]JADO Technologies GmbH, Tatzberg 47-51, 01307 Dresden, Germany. [4]Department of Chemistry, Technical University of Dresden, Bergstr. 66, 01069 Dresden, Germany. [5]Biotec, Biotechnologisches Zentrum, Tatzberg 47/49, 01307 Dresden, Germany. [6]Center of Neurological Medicine, Waldweg 33, 37073 Göttingen, Germany.

*To whom correspondence should be addressed. E-mail: simons@mpi-cbg.de

An added advantage of using a sterol as a membrane anchor is that the inhibitor not only is inserted into the membrane plane, but may also be enriched in sterol-rich domains. Cholesterol appears to be a risk factor for AD (*18*), and cholesterol-sphingolipid domains in cellular membranes, termed rafts (*6*), function as sites for the amyloidogenic cleavage of APP (*19*, *20*). β-Secretase is enriched in these microdomains (*6*, *19*, *20*). By linking the inhibitor to a sterol, we may have not only targeted it to endosomes, but also enriched the inhibitor in raft domains in these compartments. To determine whether targeting to raft domains promoted the inhibitory effect or was sufficient to simply anchor the inhibitor to the membrane, we synthesized inhibitors with different anchors—palmityl, myristyl, and oleyl (fig. S3)—with different affinities for membranes and raft microdomains (*21*). The oleyl-linked inhibitor was much less active in inhibiting β-secretase than were the saturated chains, the 18-carbon palmitate being intermediate in action between the sterol and the 14-carbon myristate (Fig. 3A).

To test whether this inhibition correlated with raft partitioning, we used scanning fluorescence correlation spectroscopy (sFCS) and avalanche photodiode (APD) imaging on supported bilayers exhibiting a raft-like liquid-ordered (lo)/non–raft-like liquid-disordered (ld) phase separation (fig. S7). Partition coefficient measurements revealed that the sterol-linked inhibitor and the palmityl-linked inhibitor partitioned into raft domains more readily than did the oleyl counterpart (Fig. 3B). Thus, raftophilic anchors of β-secretase inhibitors enhance their inhibitory potential.

To determine whether sterol-linked inhibitors were also effective in vivo, we used triple transgenic *Drosophila* expressing human wild-type APP, β-secretase, and presenilin as a model system. These flies show age-dependent neurodegeneration, a shortened life span, and semilethality and can be rescued by pharmacological treatment with secretase inhibitors (*22*). To study whether the sterol-linked inhibitor attenuated toxicity in these flies, we compared the eclosion rates of transgenic larvae that had been fed the sterol-linked inhibitor to those of solvent-treated controls (Fig. 4A). Treatment of larvae with the sterol-linked inhibitor increased survival rates; hence, the compound not only inhibited β-secretase effectively in cell culture, but also reduced toxicity in vivo. To test whether the sterol-linked inhibitor also efficiently inhibited Aβ production in mammals, we injected the inhibitor stereotaxically into the hippocampus of APPsw/PSΔE9 mice (*23*) and compared the result with mice in-

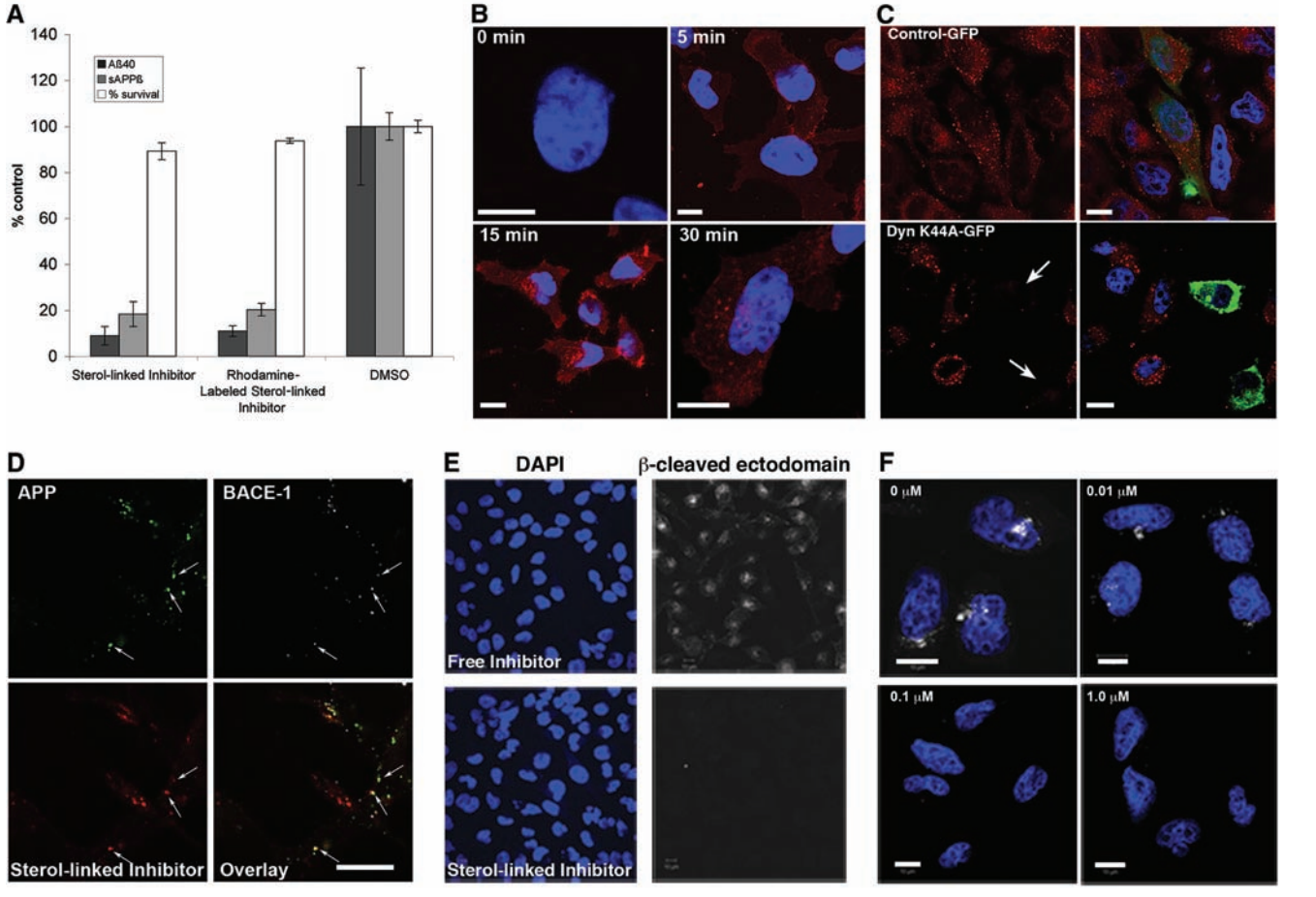

Fig. 2. Sterol-linked inhibitor is internalized into endosomes containing APP/β-secretase. (**A**) Rhodamine-labeled, sterol-linked inhibitor also inhibits β cleavage and Aβ production. Medium of HeLa-swAPP cells treated with inhibitors (2 μM) was analyzed for β cleavage, Aβ40, and cell viability (percent survival) as described for Fig. 1. Results presented are representative of three independent experiments and are expressed as means ± SD (sAPPβ, $P < 0.001$; Aβ40, $P = 0.014$). (**B**) HeLa-swAPP cells were treated with 2 μM rhodamine-labeled, sterol-linked inhibitor (red) for various times indicated. (**C**) Dynamin mutant (DynK44A-GFP), but not control GFP, inhibits internalization of the rhodamine-labeled sterol-linked inhibitor. Arrows indicate reduced internalization of the inhibitor in dynK44A-transfected cells. (**D**) Internalized sterol-linked inhibitor colocalized with internalized APP (green) and β-secretase (white) in endosomes (arrows indicate representative spots). (**E**) β-cleaved ectodomain staining in free inhibitor- or the sterol-linked inhibitor-treated cells (white) (*6*). (**F**) Cells were treated with different concentrations (inset) of the sterol-linked inhibitor as shown. Note that β-cleaved ectodomain (white) levels are already undetectable at 0.1 μM levels. DAPI (4′,6′-diamidino-2-phenylindole) staining (blue) indicates nuclei in (B), (C), (E), and (F). scale bar, 10 μm [(B), (C), (D), and (F)].

jected with either the free inhibitor or the solvent control, dimethyl sulfoxide (DMSO). The sterol-linked inhibitor was indeed more effective than the free inhibitor in inhibiting Aβ production (Fig. 4B).

Thus, membrane anchoring markedly increased the potency of a β-secretase inhibitor. By anchoring the inhibitor to the membrane, we achieved two goals: (i) The inhibitor became endocytosis-competent and gained access to endosomal β-secretase; and (ii) we reduced the dimensionality of the otherwise soluble inhibitor, thereby enhancing the interaction between the inhibitor and the enzyme (*24*). Reaction rates between solutes and membrane receptors can be enhanced by reducing the dimensionality of the solute via nonspecific adsorption (*24*), and here this model has been realized in designing drug candidates. This model also explains why such a membrane-anchored version of the inhibitor would be superior to a soluble but membrane-permeable inhibitor. If tethered molecules (e.g., the enzyme and the inhibitor) were partitioned within microdomains, both the concentration and the interaction times of the components would be increased (*25*), as we have observed. By choosing sterol as a membrane anchor, the inhibitor is enriched in the vicinity of raft-associated β-secretase, thus enhancing their interaction. The increased potency of the sterol-linked inhibitor confirms that the lipid environment and the subcellular localization of β-secretase regulate its activity (*6*, *20*). The concomitant increase in production of the neuroprotective α-cleaved ectodomain highlights the advantage of such an inhibitor, which may explain the efficacy observed in the transgenic fly model (*22*).

This work represents a proof-of-principle for a new approach in the design of more effective β-secretase inhibitors for the treatment of Alzheimer's disease. Because we used a transition-state analog against β-secretase, it was imperative to target the inhibitor to endosomes where it was active. However, this principle could also be used to design strategies to develop inhibitors against other membrane protein targets that are active at the plasma membrane and/or in intracellular compartments.

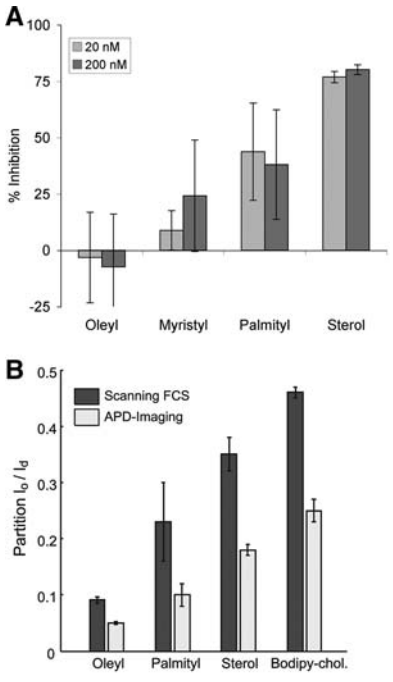

Fig. 3. Raft partitioning of inhibitors enhances their inhibitory potential. (**A**) HeLa-swAPP cells were treated with 20 nM or 200 nM test compounds for 4 hours; medium was harvested and analyzed for sAPPβ (*6*). Percent inhibition of β cleavage is shown as mean ± SD (sterol versus oleyl, $P = 0.009$). Palmityl, Myristyl, and Oleyl represent the anchor modifications of the inhibitors via palmitylation, myristylation, or oleylation, respectively. (**B**) Raft partitioning of oleyl-, palmityl-, and sterol-anchored inhibitors. Partition coefficients of inhibitors with different linkers and BODIPY-cholesterol (Bodipy-Chol.) into non–raft-like liquid disordered (ld) and raft-like liquid ordered (lo) phase were obtained by scanning FCS and APD imaging.

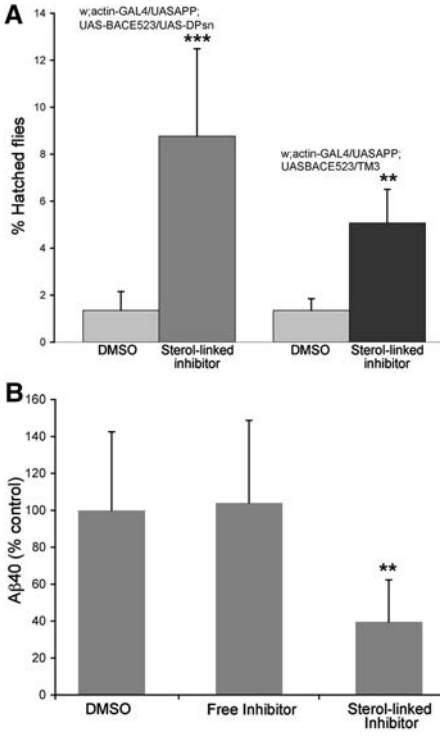

Fig. 4. Sterol-linked inhibitor rescues the lethality of transgenic flies and inhibits the production of Aβ in transgenic AD mice. (**A**) The eclosion numbers of flies, treated with either sterol-linked inhibitor (4 μM) or DMSO, were determined and their ratio versus the total amount of eclosed flies was calculated (percent hatched flies). Results are expressed as means ± SD of four experiments (**$P < 0.01$ for APP/BACE flies, ***$P < 0.001$ for APP/BACE/PRESENILIN flies; χ^2 test). (**B**) Transgenic mice were stereotaxically injected with solvent alone (DMSO), inhibitor without sterol anchor (free inhibitor), or sterol-anchored inhibitor into the hippocampus. Hippocampal Aβ levels were measured after 4 hours. Results are expressed as means ± SD of Aβ values [student *t* test; $P = 0.0068$ for free inhibitor and sterol-linked (**$P < 0.01$) and $P = 0.9389$ for DMSO and free inhibitor].

References and Notes

1. E. D. Roberson, L. Mucke, *Science* **314**, 781 (2006).
2. C. Haass, D. J. Selkoe, *Nat. Rev. Mol. Cell Biol.* **8**, 101 (2007).
3. E. H. Koo, *Traffic* **3**, 763 (2002).
4. S. A. Small, S. Gandy, *Neuron* **52**, 15 (2006).
5. A. Kinoshita *et al.*, *J. Cell Sci.* **116**, 3339 (2003).
6. L. Rajendran *et al.*, *Proc. Natl. Acad. Sci. U.S.A.* **103**, 11172 (2006).
7. X. He, K. Cooley, C. H. Chung, N. Dashti, J. Tang, *J. Neurosci.* **27**, 4052 (2007).
8. E. Kojro, F. Fahrenholz, *Subcell. Biochem.* **38**, 105 (2005).
9. W. Annaert, B. De Strooper, *Annu. Rev. Cell Dev. Biol.* **18**, 25 (2002).
10. R. Vassar, *Adv. Drug Deliv. Rev.* **54**, 1589 (2002).
11. J. S. Tung *et al.*, *J. Med. Chem.* **45**, 259 (2002).
12. L. Hong *et al.*, *Science* **290**, 150 (2000).
13. A. Capell *et al.*, *J. Biol. Chem.* **277**, 5637 (2002).
14. B. Schmidt, S. Baumann, H. A. Braun, G. Larbig, *Curr. Top. Med. Chem.* **6**, 377 (2006).
15. I. D. Hills, J. P. Vacca, *Curr. Opin. Drug Discov. Dev.* **10**, 383 (2007).
16. R. A. Nixon, *Neurobiol. Aging* **26**, 373 (2005).
17. R. Wang, J. F. Meschia, R. J. Cotter, S. S. Sisodia, *J. Biol. Chem.* **266**, 16960 (1991).
18. M. Simons, P. Keller, J. Dichgans, J. B. Schulz, *Neurology* **57**, 1089 (2001).
19. J. M. Cordy, N. M. Hooper, A. J. Turner, *Mol. Membr. Biol.* **23**, 111 (2006).
20. L. Kalvodova *et al.*, *J. Biol. Chem.* **280**, 36815 (2005).
21. M. D. Resh, *Subcell. Biochem.* **37**, 217 (2004).
22. I. Greeve *et al.*, *J. Neurosci.* **24**, 3899 (2004).
23. R. Radde *et al.*, *EMBO Rep.* **7**, 940 (2006).
24. G. Adam, M. Delbruck, in *Structural Chemistry in Molecular Biology*, A. Rich, N. Davidson, Eds. (Freeman, San Francisco, 1968), pp. 198–215.
25. B. N. Kholodenko, J. B. Hoek, H. V. Westerhoff, *Trends Cell Biol.* **10**, 173 (2000).

26. We thank G. Yu for the Hela-swAPP cells; R. Reifegerste (Evotec, Hamburg, Germany) for the transgenic flies; M. Jucker for the APPsw/PSΔE9 mice; P. Keller for help and advice with the ECL assays; V. Surendranath, W. Zacchariae, D. Lingwood, and R. Klemm for critical reading of the manuscript; and J. Bali and B. Michel for help with cell culture. Supported by Alzheimer Forschung Initiative e.V. (AFI) grant 07855 (L.R.), the European Fund for Regional Development and the State of Saxony (EFRE project 4212/06-08) (H.-J.K.), and grant 0314033 from the German Federal Ministry of Education and Research (G.J., G.S., T.B., and C.S.). K.S. is a founder of, holds equity in, and is a member of the advisory board of Jado Technologies, a company that develops novel small-molecule drugs through insights from an emerging area of cell membrane chemistry centered on rafts. H.-J.K. and G.J. are founders of and hold equity in Jado Technologies.

Supporting Online Material

www.sciencemag.org/cgi/content/full/320/5875/520/DC1
Materials and Methods
Figs. S1 to S7
References

18 February 2008; accepted 20 March 2008
10.1126/science.1156609